POLITECNICO DI TORINO
Repository ISTITUZIONALE

Evaluating the use of scrap metal to produce Al-5Cu-3Ti-1Cr-1Fe alloy powder for laser powder bed fusion

Original
Evaluating the use of scrap metal to produce Al-5Cu-3Ti-1Cr-1Fe alloy powder for laser powder bed fusion / Monti, C., Gobber, F.S., Turani, M., Papis, K., Priarone, P.C., Actis Grande, M., Bambach, M.. - In: SUSTAINABLE MATERIALS AND TECHNOLOGIES. - ISSN 2214-9937. - ELETTRONICO. - 45:(2025), pp. 1-13. [10.1016/j.susmat.2025.e01606]

Availability:
This version is available at: 11583/3002870 since: 2025-09-08T18:37:10Z

Publisher:
Elsevier

Published
DOI:10.1016/j.susmat.2025.e01606

Terms of use:

This article is made available under terms and conditions as specified in the corresponding bibliographic description in the repository

Publisher copyright

(Article begins on next page)

08 October 2026

Sustainable Materials and Technologies 45 (2025) e01606

Contents lists available at ScienceDirect

Sustainable Materials and Technologies

journal homepage: www.elsevier.com/locate/susmat

Evaluating the use of scrap metal to produce Al-5Cu-3Ti-1Cr-1Fe alloy powder for laser powder bed fusion ☆

Chiara Monti [a,b,*], Federico Simone Gobber [c], Matteo Turani [a,d], Konrad Papis [b], Paolo C. Priarone [e], Marco Actis Grande [c], Markus Bambach [a]

[a] Advanced Manufacturing Laboratory, ETH Zürich, Switzerland
[b] Materials, Processes and Sustainability, inspire AG, Zürich, Switzerland
[c] Department of Applied Science and Technology (DISAT), Politecnico di Torino, Italy
[d] Innovation Center for Additive Manufacturing, inspire AG, St. Gallen, Switzerland
[e] Department of Management and Production Engineering (DIGEP), Politecnico di Torino, Italy

ARTICLE INFO

Keywords:
Carbon footprint assessment
Aluminum alloys
Laser powder bed fusion
Gas atomization
Material recycling

ABSTRACT

This study compares the production of Al-5Cu-3Ti-1Cr-1Fe alloy powders for laser powder bed fusion (PBF-LB/M) using either virgin or recycled and scrap materials as feedstock. As for the latter, three different material sources, namely aluminum 2024, Ti-6Al-4V and AISI 316L, were selected to reproduce the target alloy composition by gas atomization. The feasibility of achieving high-quality alloyed powder from mixed scrap sources was demonstrated, with particular focus on processability, mechanical performance, and environmental impact. Both powders produced from scrap/recycled (Re-Alloy) and virgin (V-Alloy) feedstock materials were processed via PBF-LB/M to compare their printability, and the manufactured samples were tested to evaluate their mechanical properties. The Re-Alloy exhibited a stable PBF-LB/M processability over a wide set of parameters, attributed to the presence of elements like Si and Mg, which improved laser absorptivity. Mechanical testing revealed comparable properties, with the Re-Alloy achieving slightly lower strength but higher elongation at break due to the reduced Fe content. Finally, a life cycle assessment (LCA) analysis quantified the environmental impacts, showing a significant reduction of approximately 50% in the carbon footprint for the Re-Alloy powders (15.5 ± 1.0 $kgCO_2/kg$) compared to the V-Alloy (31.5 ± 1.8 $kgCO_2/kg$). The carbon footprint of the PBF-LB/M process itself was measured at 15.2 ± 1.2 $kgCO_2/kg$ of deposited material. This research highlights the potential of using recycled and waste materials to reduce the environmental impact of metal powder production while maintaining technical feasibility. The findings offer a promising approach for enhancing the sustainability of additive manufacturing processes.

1. Introduction

Aluminum alloys, known for their superior strength-to-weight ratio, corrosion resistance, and thermal conductivity, are indispensable in a wide range of industrial applications, encompassing aerospace, automotive, and construction sectors [1]. Presently, global aluminum production is estimated at approximately 100 million metric tons per year, with around 35% originating from recycled scrap and approximately 40% being lost in the manufacturing chain [2]. The dual nature of aluminum in the context of sustainability is noteworthy [3]. Firstly, its low density ($2.7\ g/cm^3$) contributes to significant fuel and energy savings in diverse applications, such as lightweight transportation, packaging, and construction, enhancing the material's appeal for sustainable development. Furthermore, its utility in electrical conduction is remarkable, achieving 64% of the conductivity of pure copper with nearly one-third the mass, attributable to its conductivity rate of 37×10^6 A/(Vm). Conversely, the production of aluminum from ore is associated with substantial greenhouse gas emissions and high energy demands, positioning it among the most environmentally impactful industrial metals [4]. This juxtaposition underscores the complexities

☆ This project was supported by Innosuisse (50175.1 IP-ENG) and the Innovation Booster Additive Manufacturing (IBAM) network. The authors thank Michael Just and Julian Hossinger from GF Casting Solutions AG for the support provided in the casting of the virgin alloy material. The authors also thank Hector Richard for the design of the watch case.

* Corresponding author at: Advanced Manufacturing Laboratory, ETH Zürich, Switzerland.
E-mail address: cmonti@ethz.ch (C. Monti).

https://doi.org/10.1016/j.susmat.2025.e01606
Received 22 February 2025; Received in revised form 30 July 2025; Accepted 13 August 2025
Available online 20 August 2025
2214-9937/© 2025 The Authors. Published by Elsevier B.V. This is an open access article under the CC BY license (http://creativecommons.org/licenses/by/4.0/).

inherent in leveraging aluminum's benefits while mitigating its environmental detriments, and this necessitates the exploration of sustainable alternatives.

The PBF-LB/M technology has revolutionized the manufacturing landscape by offering geometric freedom, allowing the optimization of lightweight components with enhanced design and functionality over their traditional counterparts [5]. Furthermore, the inherent efficiency of the PBF-LB/M process in material usage, where unmelted powder can be recycled for future builds, contrasts with subtractive manufacturing methods that generate waste by removing material to shape a component. This difference is especially pronounced in the production of complex geometries common in aerospace applications, where traditional manufacturing methods result in high buy-to-fly ratios, often exceeding 95%. The advantage of on-demand production facilitated by PBF-LB/M not only minimizes transportation within the supply chain but also curtails waste related to maintaining extensive inventories. However, a recent paper by Graziosi et al. [6] highlights how PBF-LB/M technologies still face sustainability challenges. In particular, they underscore how the reduction of material waste is context-dependent and mainly valid for parts characterized by high embodied energy or low production volumes, where the impact of machining would be important [7]. Due to the high energy to generate the laser beam, most parts produced by PBF-LB/M possess higher energy consumption per kilogram of material processed compared to casting, moulding, or extrusion [8]. In addition, the environmental impacts related to raw material production and powder atomization processing are large. Faludi et al. [9] have shown that the specific energy consumption for an efficient build of AlSi10Mg, a common aluminum alloy for additive manufacturing, on a well-utilized building platform is approximately 566 MJ/kg. When considering the energy invested in primary production, the embodied energy of bulk AlSi10Mg stands at roughly 189 MJ/kg, with the atomization process contributing an additional $\sim$ 8 MJ/kg to the material's embodied energy [10]. Consequently, a significant portion of the CO_2 footprint associated with PBF-LB/M manufactured parts originates from steps preceding the additive manufacturing process itself, underscoring the critical role of materials sources in enhancing the sustainability of this manufacturing technology. Therefore, there is a need to improve the efficiency of PBF-LB/M feedstock production to promote sustainable manufacturing. A promising strategy is to include sustainability as a performance requirement when developing materials, for instance, by designing metal alloys tolerant to impurities to enable more recycling, using recycled materials as raw feedstock, or avoiding alloying elements with unstable supply chains [11].

In this context, however, current state of the art has mainly focused on the investigation of powder reuse in PBF-LB/M and its effect on the properties of the final part. Powder that has been previously processed but not consolidated can be sieved and reused without combining it with different powders. This approach is the most frequently adopted method [2]. Alternatively, used powder can be sieved and mixed either with fresh powder or with used powder in comparable aging conditions. Cordova et al. [12] conducted a comprehensive study on the effects of powder reuse on the microstructure and mechanical behavior of Al–Mg–Sc–Zr alloys processed by PBF-LB/M. The research demonstrated that reused powder, with proper sieving and a rejuvenation step incorporating 40% virgin powder, does not significantly alter the composition or morphology compared to virgin powder, and the mechanical properties exhibited minimal differences between specimens built with virgin and reused powder. In parallel, Smolina et al. [13] explored the continuous reuse of AlSi7Mg0.6 powder in PBF-LB/M processes. The study revealed that powders and bulk samples exhibit repeatable properties through at least five consecutive PBF-LB/M processes without the addition of virgin powder, indicating the potential for a collective ageing powder reuse strategy for this alloy. However, in another study, Tradowsky et al. [14] used PBF-LB/M to create AlSi10Mg specimens, observing a significant increase in porosity from 0.26% in virgin powder specimens to 2% in those made from recycled powder without sieving, attributing this to oxide formation and noting an 8% decrease in strength and 14% reduction in elongation. Conversely, Asgari et al. [15] found no significant differences in particle size or mechanical properties between virgin and sieved recycled powders, suggesting that sieving mitigates the negative effects on part quality.

In parallel, some recent studies have moved beyond powder reuse and begun exploring the use of bulky metallic scraps or recycled solid materials as feedstock for powder production in PBF-LB/M. In contrast to the reuse of residual powders, which may only require reconditioning or re-screening, these solid materials must be re-melted and subsequently gas atomized to produce powders with the appropriate characteristics for additive manufacturing processes. For instance, Cacace et al. [16] demonstrated that recycled AISI 316L stainless steel can be successfully used to produce gas-atomized metal powders for PBF-LB/M, yielding components with comparable mechanical properties compared to those made from standard AISI 316L powders. Similarly, Benedetti et al. [17] showed that Inconel 718 powder derived from atomized metallic scrap can be used to produce components with mechanical properties comparable to those made from conventionally sourced powders, while significantly reducing carbon footprint and energy consumption by over 90%. Moon et al. [18] investigated the recycling of titanium scraps using the electromagnetic cold crucible (EMCC) method combined with calcium treatment, demonstrating a promising approach for producing high-purity titanium by effectively removing impurities, which could potentially support the development of sustainable titanium powder feedstock for additive manufacturing. These studies demonstrate the feasibility of using recycled material, but typically employ feedstock with uniform composition, simply reproducing the original alloy. This inherently limits the alloy design space to well-established and widely available scrap types.

To overcome this limitation, the present research explores an alternative strategy: reproducing a complex alloy composition by combining different scrap sources, each contributing selected alloying elements, to achieve the target chemistry. This approach enables the use of abundant and diverse scrap materials, thus promoting material circularity without being constrained to single-origin scrap or virgin feedstock. Despite its potential, this method remains largely underexplored in the context of PBF-LB/M. The aim of this research is to demonstrate a new approach to sustainable alloy design for PBF-LB/M by reproducing a complex alloy composition using a combination of diverse scrap sources, rather than relying on single-origin recycled material. This strategy enables the use of readily available metallic waste streams and supports circular material flows in additive manufacturing. The alloy Al-5Cu-3Ti-1Cr-1Fe [wt.%] developed by Monti et al. [19] has been chosen as the reference alloy. Despite it is less used in PBF-LB/M industry than other Al alloys (such as AlSi10Mg, AlSi12, Al-Mg-Sc), its high strength and the absence of critical, expensive or volatile elements, make it an optimal candidate for a study focusing on sustainability and recyclability of metal scrap. Powders have been produced from both primary and secondary feedstock. In the latter case three different material sources have been identified to be atomized to target the reference composition: a 100%-recycled aluminum 2024, a Ti-6Al-4V titanium alloy scrap, and an AISI 316L stainless steel scrap. All these three sources are known to be abundant and easily collectable [20]. The aluminum material was properly diluted with the other scrap sources during the gas atomization process and the alloyed powder was produced. Both powders underwent PBF-LB/M process to compare processability and mechanical properties. To provide a comprehensive evaluation, the study further investigated the environmental sustainability of the approach. A Life Cycle Assessment (LCA) was conducted to quantify energy demand and carbon footprint across the entire manufacturing chain, including gas atomization and additive manufacturing phases.

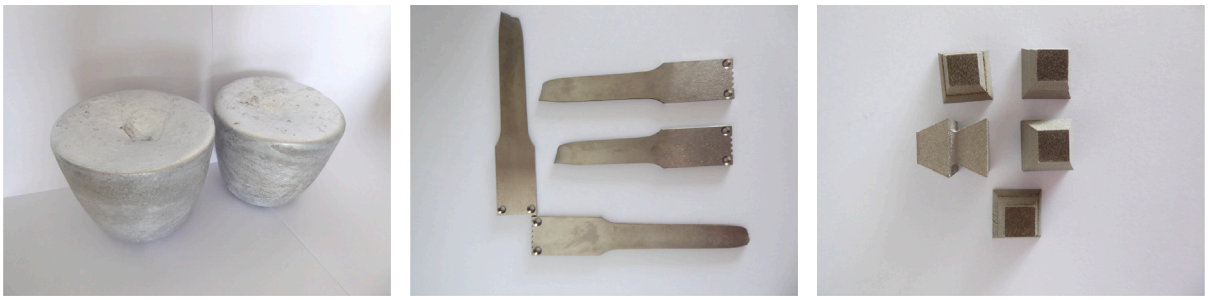

(a) (b) (c)

Fig. 1. Sources of material for the atomization of Re-Alloy: (a) recycled aluminum 2024 provided by Novelis AG; (b) Ti-6Al-4V tested tensile bars; (c) 316L stainless steel pyramids previously printed by PBF-LB/M.

Table 1
Chemical compositions of the Re-Alloy source materials measured by EDX. All the values are expressed in wt.%.

	Al	Cu	Ti	Cr	Fe	Mn	Mg	Si	Ni	V
Al2024	Bal.	4.3 ± 0.30	0.15 ± 0.01	0.1 ± 0.06	0.5 ± 0.02	0.5 ± 0.05	1.5 ± 0.10	–	–	–
Ti-6Al-4V	6.21 ± 0.10	–	Bal.	–	–	–	–	–	–	4.52 ± 0.90
316L	–	0.18 ± 0.01	–	18.21 ± 1.72	Bal.	0.32 ± 0.60	–	–	6.35 ± 1.20	–

2. Materials and methods

2.1. Master alloy production and recycled materials

Virgin material with nominal composition of Al-5Cu-3Ti-1Cr-1Fe [wt.%] was cast by GF Casting Solutions AG (Schaffausen, Switzerland) into ingots for a total mass of approximately 12 kg of material. The alloying elements were provided as base Al-5Ti [wt.%], diluted with mild steel, FeCr90 and pure copper. Recycled materials and metallic scraps employed in this study (Fig. 1) were collected from different sources. Aluminum (Al) and copper (Cu) were recovered from recycled Al2024 ingots supplied by Novelis AG (Küsnacht, Switzerland); iron (Fe) and chromium (Cr) were obtained from failed PBF-LB/M builds of AISI 316L stainless steel pyramidal specimens produced in the authors' laboratory; titanium (Ti) was sourced from previously tested Ti-6Al-4V tensile specimens. The compositions of the scrap materials and the gas-atomized powders were measured using a scanning electron microscope (SEM) EVO10 (Zeiss, Germany) equipped with an energy-dispersive X-ray spectrometer (EDX, Oxford Instrument X-Max, United Kingdom) and are reported in Table 1. The different sources were weighed and added to obtain a composition close to that of the virgin material. For the sake of simplicity, the two alloys will hereafter be referred to as V-Alloy (Virgin Alloy) and Re-Alloy (Recycled Alloy), respectively.

2.2. Atomization process

The gas atomization of the powders was performed using a Close-Coupled Vacuum Inert Gas Atomizer (CC-VIGA), model PSI Hermiga 100/10, at the facilities of Politecnico di Torino (Torino, Italy). The same melting and atomization conditions were applied for the V-Alloy and Re-Alloy to ensure comparability. The atomizer configuration followed the schematic and procedural details reported in [21], including the characterization of the energy consumption of the equipment and the accessories. High-purity Argon 5.0 served as the shielding gas during both the melting and gas atomization stages. Initially, the feedstock material was prepared by cutting it into suitable sizes, cleaning it in an ultrasonic bath, and loading it into an alumina-based crucible with a capacity of 1.25 L (Figs. 2(a) and 2(e)). The vacuum induction melting (VIM) furnace and the atomization tower were subsequently evacuated to 2 $\times 10^{-2}$ mbar to achieve the required inert atmosphere.

Induction heating was employed to gradually increase the feedstock temperature, maintaining a controlled heating rate of approximately 20 °C/min (Figs. 2(b) and 2(f)). The following induction parameters were applied: (*i*) power from 3 to 8 kW, (*ii*) frequency from 6 to 7 kHz, and (*iii*) voltage from 110 to 200 V. Once the feedstock temperature reached 400 ± 10 °C, the VIM furnace and the atomization chamber were backfilled with argon to 0.05 barg. To shield the molten bath and reduce the volatilization of light elements, a continuous argon flow was maintained within the furnace. The molten bath was subsequently overheated to 1250 °C to achieve full dissolution of alloying elements (Figs. 2(c) and 2(g)). A soaking period of 5–10 min was allowed to ensure: (*i*) proper dissolution of the Al-Ti-based intermetallic compounds and FeCr90 addition in the V-Alloy to achieve the target composition reported in Table 2; (*ii*) complete integration of AISI 316L and Ti-6Al-4V in the Re-Alloy. The pressure was raised in the melt chamber before starting atomization and set to 0.25 barg to force the flow of molten metal through the melt delivery nozzle (having a diameter of 2.4 mm) into the atomization chamber, while the measured oxygen level in the atomization chamber was below 5 ppm (Cambridge Sensotec — Rapidox 1100 Zr).

Table 2
Chemical composition in wt.% of the AlTiFeCu base ingots for V-Alloy as measured by OES before loading FeCr90, and of the gas-atomized powder measured by EDX.

	Al	Cu	Ti	Cr	Fe
Ingot	Bal.	5.21 ± 0.34	3.44 ± 0.21	0.23 ± 0.01	1.02 ± 0.02
Powder	Bal.	5.03 ± 0.18	3.03 ± 0.19	0.84 ± 0.05	1.06 ± 0.05

Argon was simultaneously injected into the gas atomization nozzle at 35 bar to initiate the atomization process, ensuring uniform particle formation. After each gas atomization, the powders collected in the primary hopper were unloaded without further passivation and stored under an inert atmosphere prior to mechanical sieving in the 20 - 63 μm range. The main atomization parameters of the two gas atomization processes for each alloy are reported in Table 3 together with the gas-to-metal mass ratio (G/M ratio) calculated from the amount of argon and metal used during the atomization. These data were considered for the carbon footprint analysis.

2.3. Powder characterization

The particle size distribution was determined by laser diffraction (Bettersizer S3 Plus, Bettersize, China). Morphology of the powders was

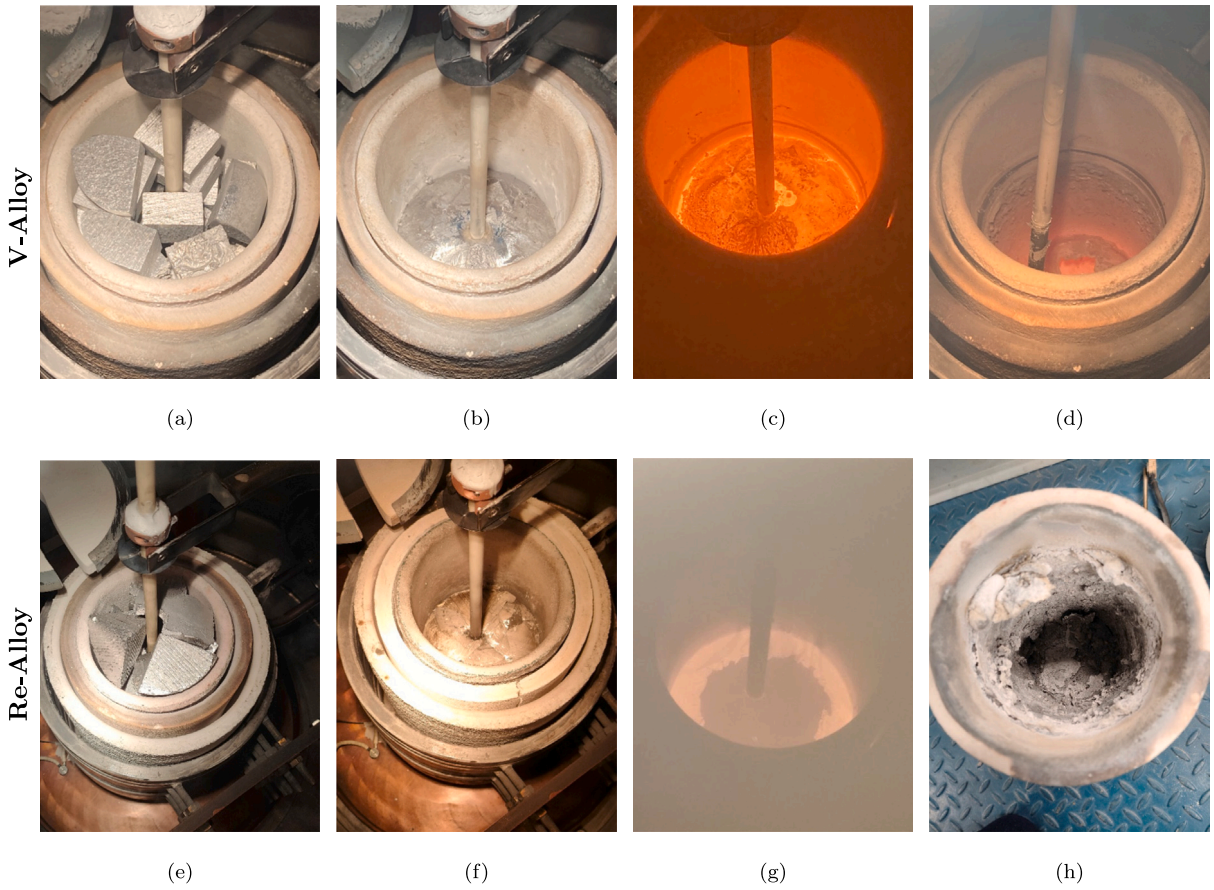

Fig. 2. Closeup of the crucible in the VIM furnace for the V-Alloy and the Re-Alloy: (a, e) loading step, (b, f) alloy melting, (c, g) overheating, (d, h) residual slag.

Table 3
Main gas atomization process parameters.

	Material loaded [kg]	$P_{atomizing}$ [bar]	$P_{melt\ chamber}$ [barg]	Melt overheating [° C]	G/M ratio
V-Alloy	2.78 ± 0.36	35	0.25	1250	2.52 ± 0.05
Re-Alloy	3.34 ± 0.08	35	0.25	1250	3.23 ± 0.03

determined qualitatively using a SEM EVO 10 at 20 kV and quantitatively on a dry sample weighting 0.02 g by static image analysis using a Malvern Morphologi with 20X magnification. The as-measured data were then treated applying a moving average with 5 μm step. The oxygen content in the gas atomized powders was measured using the Leco ONH 836 analyzer (Leco, US) according to the ASTM E1019 standard. Three repetitions per each powder were performed in the 20–63 μm particle size range and an average value was reported. The powder absorptivity spectrum was evaluated in the range of 250–1250 nm with UV–Vis-NIR spectrophotometer UV-2600 (Shimadzu, Japan) equipped with the Integrating Sphere Attachment ISR-2600Plus (Shimadzu). Cuvettes with a quartz window plate (P/N 206–89065-41 from Shimadzu) were used as powder sample holders for the analysis. A layer of powder thicker than 1 mm was measured to prevent the light interaction with the cuvette's rear surface. To evaluate the rheological properties of the powders, flowability measurements were performed on Re-alloy and V-alloy powders sieved to a particle size range of 20–63 μm and compared with a commercial AlSi10Mg powder (EOS GmbH) intended for PBF-LB/M. Flow behavior was assessed using two techniques: a Hall flowmeter test (in accordance with ASTM B213-17) and an FT4 powder rheometer (Freeman Technology). The Hall flowmeter test, conducted on a steel volume-equivalent basis using 25 g samples dried under vacuum for 8 h, provided a basic indication of free-flowing behavior. In contrast, the FT4 powder rheometer enabled a more comprehensive analysis of dynamic flow properties under low-stress conditions, representative of powder spreading in additive manufacturing processes [22]. FT4 testing followed the "Stability and Variable Flow Rate (SVFR)" standard protocol, yielding key parameters such as Basic Flow Energy (BFE) and Specific Energy (SE), which quantify the resistance to flow under stressed and unstressed conditions, respectively.

2.4. PBF-LB/M process

To optimize the manufacturing process, cubic samples with an edge of 10 mm were manufactured by PBF-LB/M on an AconityMidi+ (Aconity 3D GmbH, Germany) equipped with a single 1070 nm IPG Yb:YAG fiber laser with maximum power of 400 W and spot size adjustable between 70 and 500 μm. The process was performed in a nitrogen atmosphere. Spot size, layer thickness and hatch distance were fixed at 70 μm, 30 μm, and 110 μm, respectively. A 90° rotation scanning strategy was applied between subsequent layers. A parametric study varying the laser power P (from 300 to 370 W) and the scan speed v (800–1700 mm/s and 600–1400 mm/s for V-Alloy and Re-Alloy, respectively) was conducted to identify the combination of parameters

(a) (b) (c)

Fig. 3. Geometry of the samples used for the quantification of the power demand during the PBF-LB/M process. (a) CAD model of the watch case; (b) final printed part; (c) final build job after PBF-LB/M process.

that would enable the production of defect-free components. The density of the parts was evaluated through optical analysis. A grayscale image of the polished cross-section was captured using an optical microscope (Keyence VHX 7000, Japan). The image was then converted into binary format using a custom MATLAB script. The optical density was determined by calculating the ratio of black pixels to the total number of pixels within a user-specified region of interest.

Tensile specimens with a final geometry in accordance with DIN 50125 were obtained from raw cylinders (L = 80 mm, D = 8 mm) produced with their long axis aligned to the building direction and using the parameters optimized for the highest density (P = 370 W, and v = 800 mm/s and 1400 mm/s for V-Alloy and Re-Alloy, respectively) and then machined. Room-temperature uniaxial tensile tests were performed on a 25-kN tensile testing machine walter+bai LFV-25kN HH (walter+bai AG, Switzerland). Strain-controlled tests were carried out at a speed of 1 mm/min. Five samples per each alloy were tested and the tensile values were reported as mean values and standard deviations.

To evaluate the energy consumption during the PBF-LB/M process for the LCA, two different jobs consisting of 17 watch cases (Figs. 3(a) and 3(b)) were manufactured using the V-Alloy and the Re-Alloy. During the printing process, the power demand of the machine was measured using an HIOKI 3196 power quality analyzer (HIOKI E.E. Corporation, Japan). This case study was selected as it represents a realistic full-build job, as shown in Fig. 3(c), making it suitable for assessing energy demand in practical manufacturing scenarios.

2.5. Carbon footprint assessment

The methodology employed for the carbon footprint assessment is based on the principles of LCA, in accordance with the ISO 14040/44 standards [23,24], the ISO 14067 standard [25], and the guidelines set forth by the Joint Research Center (JRC) of the European Commission [26,27]. LCA is widely applied to cradle-to-gate or cradle-to-grave studies involving additive manufacturing (AM) processes and their associated pre- and post-manufacturing operations, as reviewed by Pusateri et al. [28]. The aim and scope of this analysis is to quantify and compare the carbon footprint of gas atomized powders with varying proportions of input materials loaded into the atomizer (ranging from bulky scrap to metal feedstocks with differing recycled contents), and to ascertain the extent to which this impact affects the carbon footprint of the PBF-LB/M process. The system boundaries are defined as cradle-to-gate, and the selected metric for the environmental impact assessment is the amount of equivalent carbon dioxide (CO_2) emissions. The unit processes and the main material flows are schematized in Fig. 4.

First, the analysis was conducted on a single unit mass (1 kg) of AM powder within the 20–63 μm range, which was assumed as the functional unit (i.e., the system boundary labeled "A", encompassing the production of raw materials and the manufacturing of the powder, was considered). Secondly, the PBF-LB/M was included in the assessment (system boundary "B") to verify whether the carbon footprint of AM-ed parts is predominantly influenced by the materials, atomization, or the PBF-LB/M process, particularly when utilizing a different powder feedstock.

Table 4
Granulometric indicators for V-Alloy and Re-Alloy powders.

Indicator	V-Alloy	Re-Alloy
D_{10} [μm]	20.6	21.2
D_{50} [μm]	34.9	36.7
D_{90} [μm]	58.6	59.8
Span	1.10	1.11

3. Results

3.1. Powders characterization

The particle size distribution (PSD) of the V-alloy and Re-alloy is shown in Fig. 5 and the respective granulometric indicators in Table 4. The D_{50} values, representing the median volumetric particle size, are measured to be 34.9 μm and 36.7 μm for V-Alloy and Re-Alloy, respectively. Some fine particles with D ≤ 20 μm remain after sieving due to the cohesive forces between them. Nevertheless, the two particle size distributions are largely comparable. The SEM images in back-scattered electron (BSE) mode in Figs. 6(a) and 6(b) provide a visual representation of the powder particles. The particles appear predominantly spherical, although some irregular-shaped particles can also be observed. The composition of the powders, obtained by EDX analysis, is summarized in Table 5. Interestingly, the Mg content in the Re-Alloy powders was significantly lower than in the recycled Al2024 feedstock material (Table 1). This depletion is attributed to the high volatility of Mg in the absence of protective fluxes [29], as expected in the VIM process used.

Fig. 7 shows the morphological indicators of circularity and convexity as a function of particle size for the investigated powders. As expected, the morphological quality decreases with increasing particle size. This trend is particularly evident beyond 40 μm and is likely due to the higher probability of shape deviation from sphericity due to a higher tendency to impingement with solidifying particles in the atomization plume. The V-Alloy and Re-Alloy powders display comparable trends for both circularity (Fig. 7(a)) and convexity (Fig. 7(b)), reflecting the shared gas-atomization unit and process parameters used in their production. In contrast, the commercial AlSi10Mg powder exhibits a slightly lower morphological quality, particularly in terms of convexity, which may be attributed to a higher incidence of satellites or surface imperfections. This implies that powders can appear generally spherical, yet still possess rough or irregular surfaces that may affect flowability and packing density. The rheological tests revealed significant differences in flow behavior between the three compared powders

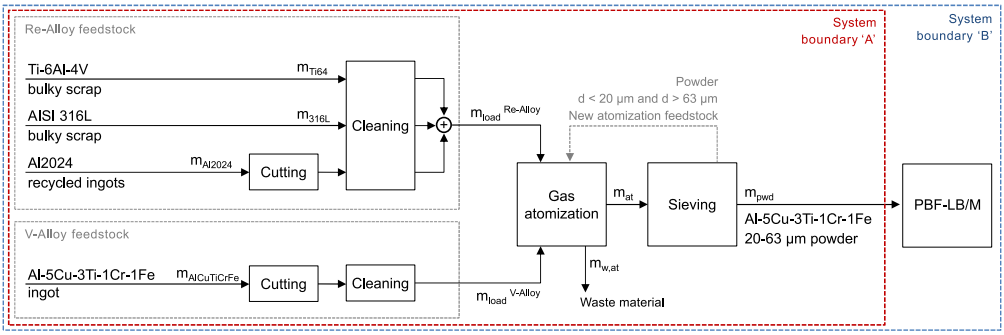

Fig. 4. System boundaries for the LCA, highlighting the two different material inputs for Re-Alloy and V-Alloy powder production.

Table 5
Chemical compositions of the V-Alloy and Re-Alloy powders measured by EDX. All the values are expressed in wt.%.

	Al	Cu	Ti	Cr	Fe	Mn	Mg	Si	V	Ni
V-Alloy	Bal.	5.03 ± 0.18	3.03 ± 0.19	0.84 ± 0.05	1.06 ± 0.05	–	–	0.39 ± 0.05	–	–
Re-Alloy	Bal.	4.47 ± 0.15	3.15 ± 0.27	0.14 ± 0.03	0.62 ± 0.04	0.52 ± 0.04	0.17 ± 0.06	0.17 ± 0.02	0.02 ± 0.01	0.10 ± 0.03

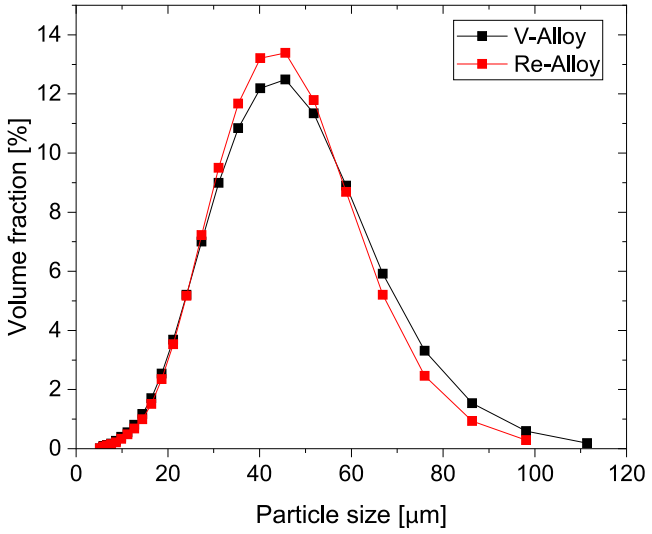

Fig. 5. Particle size distribution curves for V-Alloy and Re-Alloy powders.

Table 6
Rheological properties and flowability indicators for V-Alloy, Re-Alloy, and AlSi10Mg powders.

Property	V-Alloy	Re-Alloy	AlSi10Mg
BFE [mJ]	216.90	155.65	167.77
SI	1.01	0.99	0.95
FRI	1.11	1.16	1.06
SE [mJ/g]	2.12	1.90	2.34
CBD [g/ml]	1.72	1.63	1.49
Hall flowability [s]	21.82	16.01	19.01

(V-Alloy, Re-Alloy, and AlSi10Mg), specifically in terms of Basic Flowability Energy (BFE) and Specific Energy (SE), as shown in Fig. 8 and Table 6. Re-Alloy powder exhibited the lowest SE, indicating the least resistance to flow under low stress conditions, which is representative of the environment experienced during the recoating step in powder-bed fusion processes [30]. Slightly higher SE values were recorded for both the V-Alloy and the AlSi10Mg benchmark powder. The SE values for AlSi10Mg are consistent with those reported in the literature [22], confirming its known moderate flowability. Despite these differences, all three powders were able to flow through a Hall flowmeter funnel, and the qualitative flow behavior observed was in good agreement with the quantitative ranking obtained from the rheological measurements.

Absorbance values were measured for both V-alloy and Re-alloy powders and the results are shown in Fig. 9. The values for the Re-Alloy powder are much higher than the V-Alloy powder at every wavelength measured. The absorbance measured at 1070 nm, corresponding to the laser wavelength used in PBF-LB/M processes, was 53% for V-Alloy and 74% for Re-Alloy. This represents a 21% increase in absorbance for powders derived from scrap feedstock. The absorbance of Re-Alloy powders is higher than that of highly-processable AlSi10Mg powders (e.g., 66% as measured by Brandau et al. [31]) and significantly higher than that of other Al-Cu-based powders, such as AA 2618 (e.g., 52% as measured by Ceroni et al. [32]). The comparable PSD and morphological quality between the V-Alloy and the Re-Alloy powders suggests that the differences observed in terms of both the optical and the rheological properties should be investigated in terms of chemical surface properties.

3.2. Processing window analysis

A parameter study was conducted on both the alloys to determine the printing parameters for achieving an optimized density. Fig. 10 shows how the different absorptivity measured affects the powders processability. The V-Alloy processed with 370 W and 800 mm/s shows the highest value of density of 99.82%. The cross sections of the parts with the lowest density exhibit porosity primarily caused by lack of fusion, evident from the characteristic drop-shaped porosity pattern along the horizontal axis, and consistent with the fact that they were produced with the fastest scanning parameters. Small, round pores can be identified as gas porosity. On the other hand, the Re-Alloy shows a wider processing window, with densities higher than 99.8% achieved almost across the entire range, with the highest density of 99.97% achieved at 370 W and 600 mm/s. However, to optimize the processing time and built rate, the chosen parameters for the manufacturing of the tensile samples were 370 W and 1400 mm/s, given a satisfactory measured density of 99.90%.

An EDX measurement was also performed on the printed parts to compare their composition with that of the original powders. The results are shown in Table 7.

3.3. Tensile properties

Tensile curves for V-Alloy and Re-Alloy are shown in Fig. 11 and the values of yield strength, ultimate tensile strength (UTS), elongation

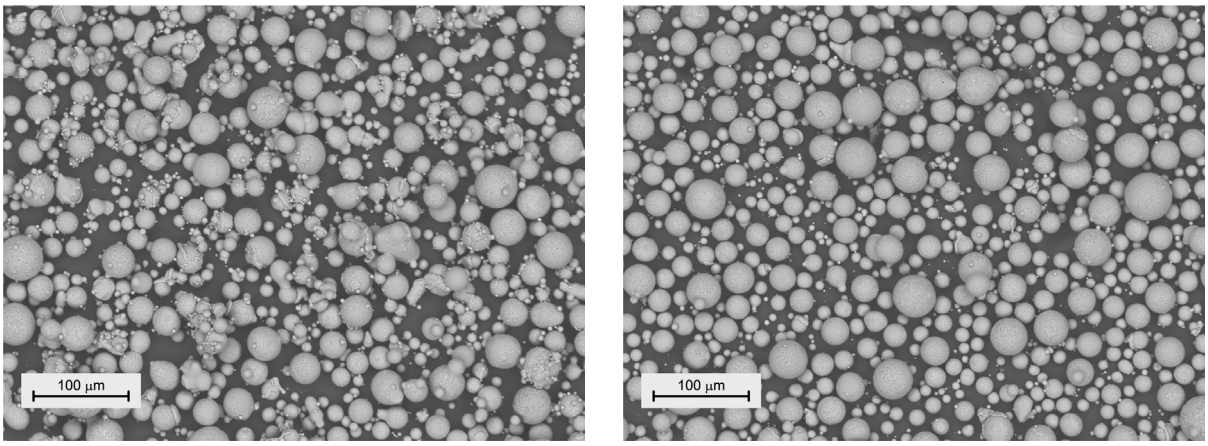

(a) (b)

Fig. 6. SEM-BSE micrographs of the investigated powders: (a) V-Alloy; (b) Re-Alloy.

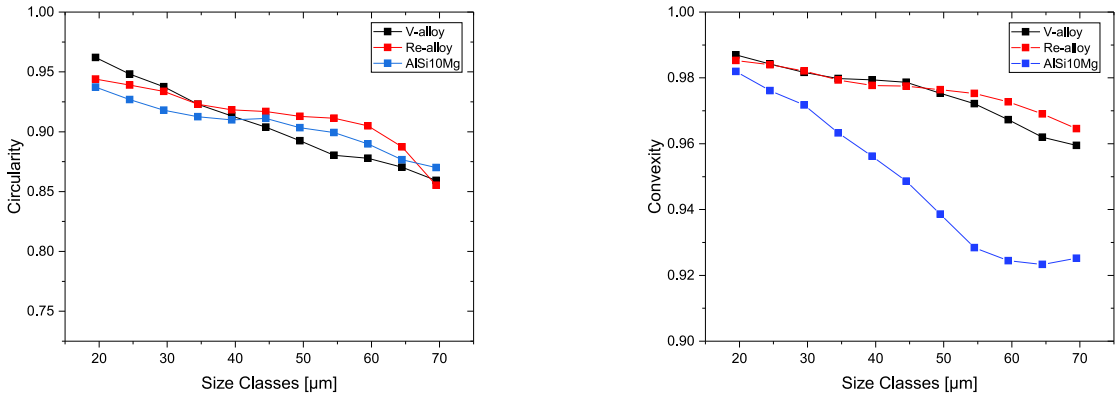

(a) (b)

Fig. 7. Morphological characteristics of the investigated powders: (a) circularity; (b) convexity.

Table 7
Chemical compositions of the V-Alloy and Re-Alloy parts measured by EDX. All the values are expressed in wt.%.

	Al	Cu	Ti	Cr	Fe	Mn	Mg	Si	V	Ni
V-Alloy	Bal.	5.23 ± 0.18	3.11 ± 0.12	0.82 ± 0.02	1.02 ± 0.03	–	–	0.10 ± 0.05	–	–
Re-Alloy	Bal.	4.38 ± 0.06	3.39 ± 0.04	0.16 ± 0.01	0.60 ± 0.03	0.57 ± 0.02	0.08 ± 0.01	0.32 ± 0.02	0.02 ± 0.01	0.11 ± 0.04

Table 8
Mechanical properties of V-Alloy and Re-Alloy.

	Yield strength [MPa]	UTS [MPa]	Elongation to fracture [%]	Elastic modulus [GPa]
V-Alloy	438 ± 6	520 ± 8	4.2 ± 0.5	70 ± 2
Re-Alloy	399 ± 10	489 ± 15	6.8 ± 2.4	68 ± 1

at break, and elastic modulus are reported in Table 8. Re-Alloy reports a yield strength close to the V-Alloy, only ca. 40 MPa smaller, while achieving an higher elongation. The fracture surfaces analyzed by SEM are reported in Fig. 12. Both surfaces show typical microvoids of a ductile fracture.

3.4. Carbon footprint results

In accordance with the stated aim and scope, system boundaries, and main assumptions (Section 2.5), the carbon footprint was quantified as a function of the data inventory detailed in the following subsections.

3.4.1. Material flows

The gas atomization process received a variety of material inputs, including (*i*) metal feedstock derived from primary and/or secondary material production and (*ii*) bulky scraps. A summary of the material flows for each atomization test is provided in Table 9. The atomization (gross) yield value, y_{AT}, defined here as the ratio of the mass of powder collected in both the primary and secondary hoppers, regardless of size, to the mass of material loaded into the crucible, m_{load}, exhibited a range of 96 to 98%. This ratio quantifies the material loss that occurs during the atomization process, which can be attributed to three main factors: vaporized material, fine dust trapped within the atomizer chamber and filters, and slag adhered to the crucible. When considering solely the proportion of powders within the 20–63 µm range that were collected

Table 9
Material flows for Re-Alloy and V-Alloy powder production.

Test ID	Re-Alloy #1	Re-Alloy #2	V-Alloy #1	V-Alloy #2
Total mass loaded into the atomizer, m_{load} [kg]	3.42	3.25	3.14	2.41
Mass of Al2024 100%-recycled ingot, m_{Al2024} [kg]	3.29	3.13	–	–
Mass of Ti-6Al-4V bulky scrap, m_{Ti64} [kg]	0.11	0.10	–	–
Mass of AISI 316L bulky scrap, m_{316L} [kg]	0.02	0.02	–	–
Mass of Al-5Cu-3Ti-1Cr-1Fe ingot, $m_{AlCuTiCrFe}$ [kg]	–	–	3.14	2.41
Mass of powder collected in the primary hopper [kg]	3.17	3.07	2.83	2.21
Mass of powder collected in the secondary hopper [kg]	0.13	0.11	0.21	0.15
Mass of powder collected after atomization, m_{at} [kg]	3.30	3.18	3.04	2.36
Atomization (gross) yield, $y_{AT} = m_{at}/m_{load}$ [%]	96.5	97.8	96.8	97.9
Mass of 20–63 μm powder collected after sieving, m_{pwd} [kg]	1.78	1.51	1.33	1.25
AM yield, $y_{AM} = m_{pwd}/m_{load}$ [%]	52.0	46.6	42.3	51.8

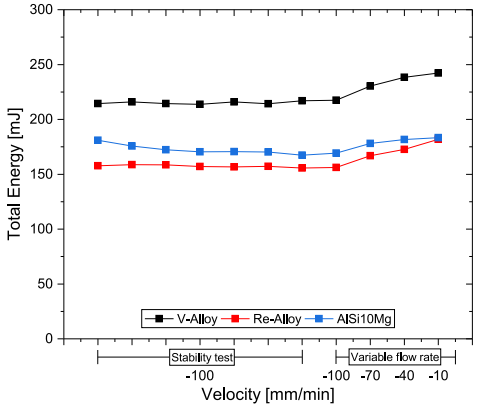

Fig. 8. Rheological properties of the powders as measured by shear cell rheometry.

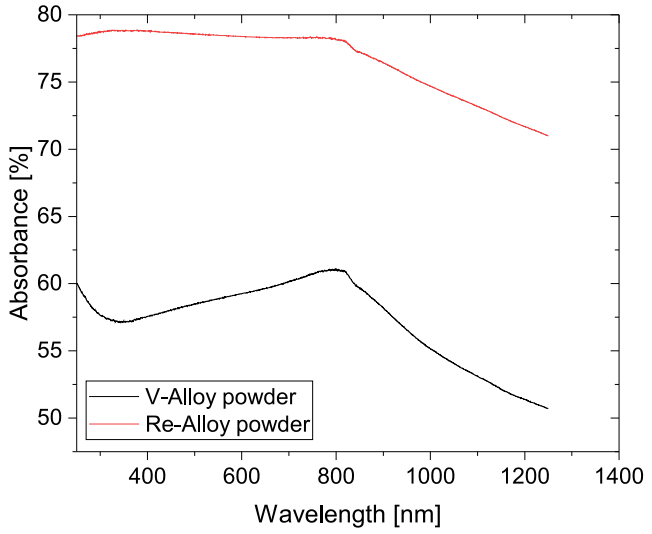

Fig. 9. Typical absorbance values for the V-Alloy and Re-Alloy powders.

for the PBF-LB/M process, the AM yield value, y_{AM}, was reduced to a range of 42%–52%. No significant differences were observed between the two process conditions for Re-Alloy and V-Alloy. The discrepancies between the replicates can be attributed to the inherent variability of the atomization process.

3.4.2. Modeling of recycling benefits

Recycling practices give rise to allocation issues because the environmental impacts associated with the unit processes involved in the extraction and processing of raw materials, as well as the final disposal of products (including recycling), are shared by the product systems that supply and receive the recycled material [25]. Consistent with the established system boundaries, the recycled content (100:0) approach was used in this analysis. Consequently, the benefits of material recycling were assumed to be contingent upon the displacement of virgin (primary) materials by recycled or scrapped materials. The sole environmental burden associated with secondary raw materials was that pertaining to the process utilized for their recycling.

In the case of Re-Alloy powder production, the carbon footprint of 100%-recycled Al2024 ingots was assumed to be 2.6 ± 0.1 $kgCO_2/kg$, according to the CES Selector database [33]. For the Ti-6Al-4V and AISI 316L bulky scraps, the impact of producing the input material that results in the scrap was allocated to the product system that generates the scrap itself. Therefore, the scraps were categorized as a *pre-consumer recycled content*, in accordance with the specifications outlined in Section 4.4.8.8 of Ref. [27].

In the case of V-Alloy powder production, due to the lack of primary and secondary data, the carbon footprint of the Al-5Cu-3Ti-1Cr-1Fe ingot material was estimated at 8.6 ± 0.7 $kgCO_2/kg$, assuming Al2024 as a proxy material and considering a recycled content in the actual material supply of $43 \pm 2\%$ [33]. The present study did not consider the potential for a closed loop associated with the recirculation of off-specification powders [17], in line with the experimental design.

Table 10
Electrical energy requirements (in kWh) for the powder production.

Unit Process	Re-Alloy #1	Re-Alloy #2	V-Alloy #1	V-Alloy #2
Cutting	0.50	0.48	1.13	0.87
Cleaning	0.06	0.06	0.06	0.06
Atomization	50.0	47.4	51.6	49.1
Sieving	0.60	0.58	0.56	0.43

3.4.3. Powder production data

Table 10 presents a summary of the electrical energy requirements of the unit processes involved in powder production. The Al-5Cu-3Ti-1Cr-1Fe and the Al2024 ingots were preliminarily cut to a suitable size to allow for insertion into the crucible. This step was not necessary for the bulky Ti-6Al-4V and 316L stainless steel scraps, which already had compatible dimensions. The 1.4 kW-rated cut-off machine was used for 21 and 43 min, respectively, for the Al2024 and Al-5Cu-3Ti-1Cr-1Fe ingots, due to the different dimensions of the feedstock. Besides electricity (Table 10), it was assumed that (*i*) material losses during cutting, (*ii*) cutting blade consumption, and (*iii*) lubricant consumption would be negligible. All batches of materials loaded into the atomizer underwent an ultrasonic cleaning treatment. This resulted in an electrical energy demand of 0.06 kWh/batch and a consumption of 0.5 kg/batch of an acetone-based solvent having an assumed carbon footprint of 2.0 ± 0.6 $kgCO_2/kg$ (see also [34,35]).

The gas atomization process, inclusive of the contributions from the inductor, vacuum pump, and chiller, required 50 ± 3 kWh/atomization, exhibiting no notable discrepancies between the tests. With regard to consumables, the contribution of crucibles and other refractory

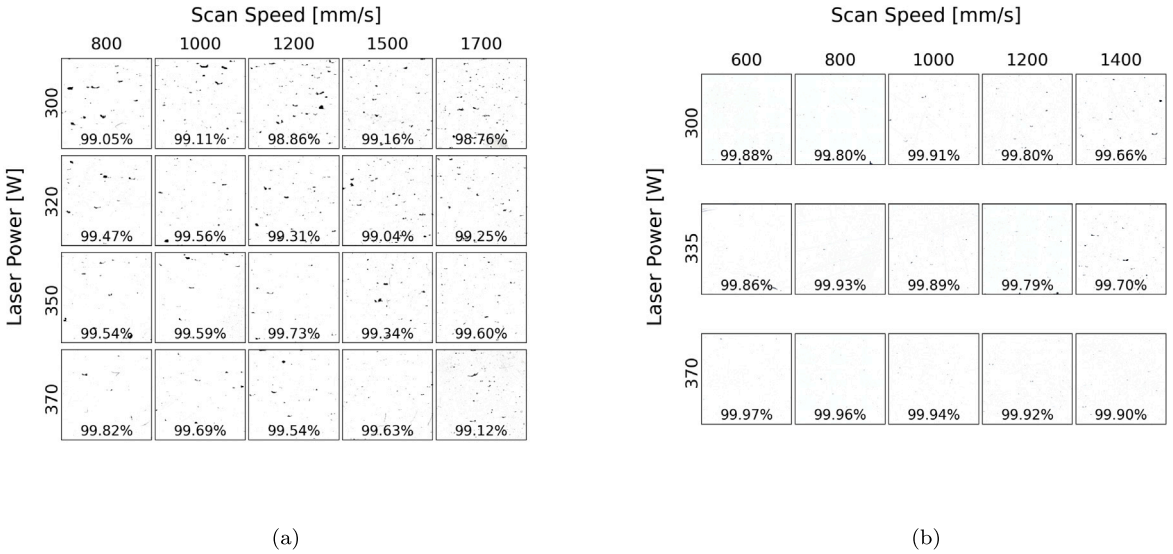

Fig. 10. Parameters study on the (a) V-Alloy and (b) Re-Alloy. Relative density is expressed as a function of laser power and scan speed at constant hatch distance of 110 μm.

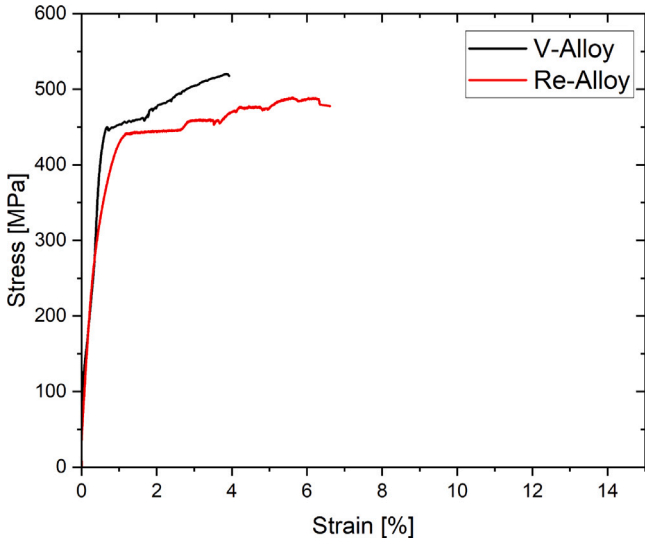

Fig. 11. Typical tensile curves for V-Alloy and Re-Alloy.

materials to the carbon footprint was quantified at 3.32 ± 0.17 $kgCO_2$ for each atomization cycle, maintaining the assumptions presented in Ref. [21], as the experimental setup was identical. In this case, the crucible replacement after three atomization cycles is a consequence of the high melting temperatures of the alloy under investigation, which exceed those of other aluminum alloys. The cleaning of the crucible to remove slag and material adhered to the walls had a negligible impact, given that it was done manually and without the use of power tools. The cleaning of the atomizer with acetone-based solvents was unchanged from Ref. [21], resulting in an additional contribution of 0.40 $kgCO_2$/atomization cycle. For sieving, only the energy consumption of the 1.1 kW-rated industrial sieve was taken into account and totaled as per Table 10.

3.4.4. Carbon footprint of powder production

Cradle-to-gate CO_2 emissions were quantified for each atomization test and the results were then related to the unit mass of powder produced in the 20–63 μm range, as shown in Fig. 13. In order to convert

Table 11
Electrical energy and resource requirements for PBF-LB/M.

Parameter	Re-Alloy	V-Alloy
Electrical energy demand, printing phase [kWh]	1.52	1.76
Electrical energy demand, total [kWh]	1.89	2.17
Manufacturing time, printing phase [h]	6.50	6.63
Manufacturing time, total [h]	9.64	9.50
Gas (nitrogen) consumption [kg]	2.67	2.43
Deposition rate [kg deposited/h]	$1.05 \cdot 10^{-2}$	$1.03 \cdot 10^{-2}$
Specific energy consumption [kWh/kg deposited]	27.8	31.9
Specific gas consumption [kg/kg deposited]	39.3	35.7

electricity consumption into CO_2 emissions, the GHG emissions intensity of electricity generation was considered to be 0.210 $kgCO_2$/kWh, assuming the EU-27 average value for the year 2023 [36].

On average, values of 15.5 ± 1.0 $kgCO_2$/kg of Re-Alloy powder and 31.5 ± 1.8 $kgCO_2$/kg of V-Alloy powder were obtained. The results for the powder production process alone (limited to cutting, cleaning, atomization, and sieving) are comparable between the test replicates and are related to the AM yield factor (Table 9). It can be observed that the increase in y_{AM} is associated with the expected reduction in the carbon footprint per unit mass of powder. The main driver contributing to the differences between the two test conditions is the impact of the loaded material, which is a consequence of the varying carbon footprints of the incoming feedstock materials (see Section 3.4.2).

3.4.5. Carbon footprint of PBF-LB/M

In order to evaluate the environmental impact of the powders in comparison to that of the additive manufacturing process, the Re-Alloy and V-Alloy powders were used to produce jobs consisting of 17 identical watch cases, with a theoretical build volume of 23.9 cm^3, as described in Section 2.4. The power versus time curves (Fig. 14) and the nitrogen consumption during the AM process were experimentally recorded and are presented in Table 11. The CO_2 equivalent emissions of the PBF-LB/M process were calculated by considering an emission factor for electricity of 0.210 $kgCO_2$/kWh, consistent with the data presented in Section 3.4.4. A carbon footprint of 0.24 ± 0.03 $kgCO_2$/kg nitrogen was assumed based on primary data obtained from the gas supplier. Based on this data set, the specific carbon footprint of the PBF-LB/M tests was comparable, amounting to 15.2 ± 1.2 $kgCO_2$ per kg of deposited material, for both tests.

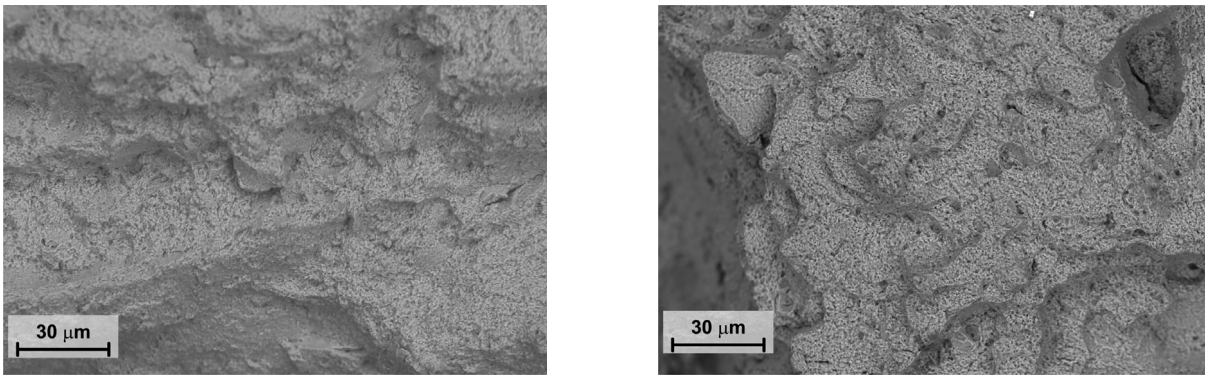

Fig. 12. Fracture surfaces of (a) V-Alloy and (b) Re-Alloy. The presence of microvoids highlights the ductile fracture for both alloys.

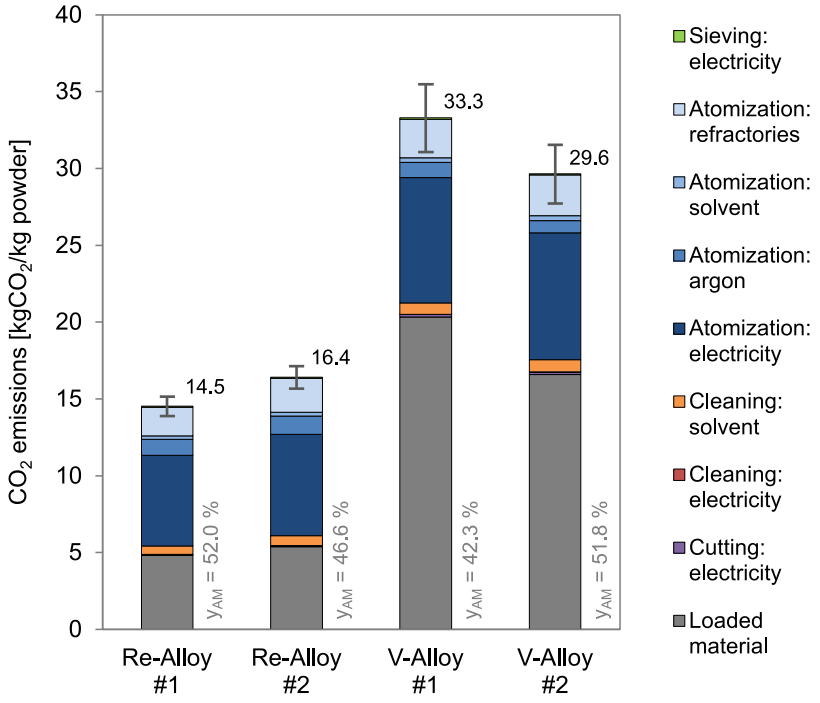

Fig. 13. Cradle-to-gate equivalent CO_2 emissions for Re-Alloy and V-Alloy powders as a function of the test conditions.

The specific energy consumption (SEC), including all pre- and post-printing phases (see Fig. 14), was quantified to be 100–115 MJ/kg of deposited material. These values fall within the range of 83–588 MJ/kg for PBF-LB/M reported in the review by Kellens et al. [37]. However, it should be noted that SEC is affected by several factors, including the size and type of AM machine, the efficiency of build volume utilization, and the deposition rate, and comparisons among the available literature data should be made with due caution.

4. Discussion

4.1. Influence of the source material on processability and mechanical properties

As expected, Re-Alloy powders produced by gas atomization of recycled and scrap material show deviations from the chemical composition of the V-Alloy. Due to the high Mg content in the Re-Alloy feedstock for powder production (Table 1), consistent evaporation was observed during melting (Fig. 2(g)). Nevertheless, the remaining Mg, along with Si and Mn, acts as a potent oxide former. A slight increase in oxygen content was measured by Leco ONH analysis for the Re-Alloy powders (0.068 ± 0.024 wt.%) compared to V-Alloy powders (0.048 ± 0.013 wt.%) in the same PBF-LB/M particle size range. Since both powders were analyzed immediately after atomization, this result reflects a difference in oxygen content in the as-atomized state. The absorbance data reveal that the presence of oxides at the surface significantly affects the absorptivity of the two powders, which is reflected in the better processability of the Re-Alloy compared to the V-Alloy. The influence of Si and Mg on the processability of Al alloys via PBF-LB/M has already been studied by Ghasemi et al. [38]. In their study, they compared the processability of pure Al, AlSi12, and AlSi10Mg, focusing on how powder absorptivity and oxygen content affect the processing window. Their findings demonstrated that the addition of Si and Mg increases the processing window for Al by enhancing the laser absorptivity of the powder material. In the case of Re-Alloy, this mechanism is believed to contribute to the enlarged processing window compared to the V-Alloy.

Despite the detection of Mg and O signals through EDX on the surface of the Re-Alloy powder, the Mg content in the PBF-LB/M parts is negligible (Table 7). This is believed to be due to a mechanism

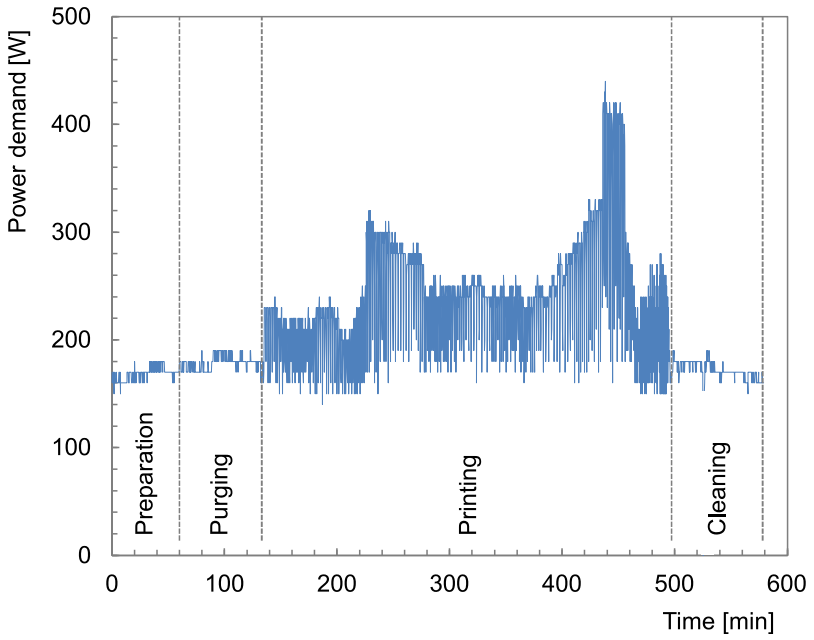

Fig. 14. Power versus time curve for PBF-LB/M using Re-Alloy powders.

similar to that influencing processability, as proposed by Ghasemi et al. [38], and based on observations of keyhole formation by Cunningham et al. [39]. During the interaction between the powder and the laser, the oxide shells separate from the powder particles, introducing numerous nano-oxides into the melt pool. These oxides then evaporate due to the high laser temperature, explaining their absence in the solidified material. However, the initial interaction between the oxide shells on the powder particles and the laser increases the powder absorptivity, thereby improving the material processability. Given that Mg and Si are common additions to conventional alloys, their presence as impurities in this case can be beneficial for enhancing processability, reinforcing the concept of using scrap for powder production.

Despite the improved processability, the tensile and yield strength of the Re-alloy are slightly lower compared to the ones of the V-alloy (see Table 8). This can be linked to the lower content of elements forming strengthening precipitates (i.e., Cu, Fe) and elements contributing to solid solution strengthening (i.e., Cr) [40]. In contrast, the Re-Alloy shows a higher elongation at break, and this can be explained by the presence of Mn (approximately 0.5 wt.%), sourced mainly from Al2024. Mn is reported to be a stabilizer of the metastable $Al_6(Fe,Mn)$, which is less critical for materials ductility than the stable $Al_{13}Fe_4$ [41,42].

4.2. Influence of the source material on carbon footprint

The analysis of CO_2 equivalent emissions showed a significant reduction (up to approximately 50%) in the carbon footprint of the powders, from 31.5 ± 1.8 $kgCO_2/kg$ for the V-Alloy to 15.5 ± 1.0 $kgCO_2/kg$ for the Re-Alloy (Section 3.4.4), entirely due to the use of scrap and/or secondary materials as atomization feedstock. In addition to reducing emissions from the source materials, further improvements are expected if higher atomization yields are achieved. This may be accomplished by optimizing the choice of process parameters as a function of the AM powder range target [21], or by using over- and undersized aluminum powders for other manufacturing processes, such as directed energy deposition [43], cold spray [44], binder jetting [45], or compression molding [46]. Furthermore, given that the carbon footprint of powders is also significantly influenced by the electricity demand during the gas atomization process, additional reductions could be achieved by decarbonizing the electricity generation [36]. The findings of this study are consistent with those of other research in this field. The energy demand of the gas atomization process for the production of aluminum powder (irrespective of particle size) has been determined to be between 15 and 20 kWh/kg. For the powder size range of 20–63 μm, this value has been observed to increase to 28–40 kWh/kg. Similar values for gas atomization processes are given by Martin et al. [47], and references therein, who mentioned a use of 11.5 kWh/kg for aluminum powder production, further increasing to values above 50 kWh/kg (leading to emissions higher than 25 $kgCO_2/kg$ of AM powder) when over- and under-sized particles are discarded and typical yields of < 20–40% are considered. Furthermore, although the results presented here are derived from laboratory-scale experiments, the carbon footprint of V-Alloy powder is comparable to the cradle-to-gate estimated CO_2 emissions of 28.8 $kgCO_2/kg$ of AM powder from gas atomization produced by a 0%-recycled aluminum alloy from industry [48]. With regard to the PBF-LB/M process, the carbon footprint results were found to be 15.2 ± 1.2 $kgCO_2$ per kilogram of deposited material. No significant differences were observed between the tests conducted with the two powders. Therefore, if the cradle-to-gate boundaries were to be extended by including the production of AM-ed components, the carbon footprint attributable to the production of powders would be comparable (in the case of Re-Alloy) or dominant (in the case of V-Alloy) to that of the additive manufacturing process itself.

It is worth noting that the results obtained here are limited to the case study considered, the modeled assumptions, and the data inventory. Therefore, the conclusions should be generalized with careful consideration. In this Life Cycle Assessment (LCA), the 100:0 approach, which follows a cut-off methodology, was applied. Under this approach, bulky scraps enter the system with zero impact, as they originate from external systems, and only the impacts of sorting, cleaning, and processing are considered. Similarly, the impact of 100%-recycled materials is limited to the remelting and reprocessing required to obtain the recycled material itself. Moreover, one of the limitations is the use of secondary data for estimating the carbon footprint of input materials. If material impacts are allocated differently, or other carbon footprints are considered, the differences in the results could be significant. Nonetheless, the recovery of waste materials for the production of powder feedstock appears to be a potentially beneficial strategy for enhancing the environmental sustainability of AM. This is particularly relevant given the well-documented limitations related to the specific

energy consumption of AM, which could be one or even two orders of magnitude higher than that of more conventional manufacturing approaches [37].

The results of this study align with previous research demonstrating the technical feasibility of producing powders from homogeneous pre-consumer scrap [17,21] or single-alloy recycled material [16], often achieving properties comparable to those of powders derived from primary resources. Where environmental assessments were carried out, these approaches also exhibited significantly reduced carbon footprints, primarily due to the minimal upstream burdens associated with scrap input. In contrast, the present research addresses a more complex scenario by employing a mixed-waste charge comprising different scrap sources and a fraction of recycled material. This approach could enable a broader assessment of how input variability influences both environmental impact and alloy performance, thereby contributing to the discussion on realistic pathways toward material circularity in additive manufacturing.

5. Conclusions and outlook

This study demonstrates the feasibility and benefits of using both recycled and scrap materials for the production of powders suitable for the PBF-LB/M processes. The following key findings have been established:

- The successful production of Al-5Cu-3Ti-1Cr-1Fe alloy powders using recycled and scrap sources (Al2024, Ti-6Al-4V, and AISI 316L) highlights the potential of reproducing complex alloy compositions from readily available scrap materials. It is acknowledged that the use of heterogeneous scrap may constrain compositional control, particularly when precise alloy specifications or narrow tolerances are required. However, this limitation can be addressed through careful charge design and, if necessary, additional refining or adjustment steps prior to atomization.
- The Re-Alloy exhibited a wider processing window during PBF-LB/M compared to the V-Alloy. This enhancement is attributed to the presence of impurities, such as Si and Mg, which improve laser absorptivity by forming oxides on the powder particles.
- The comparison of mechanical performance revealed that, although the Re-Alloy exhibited slightly lower yield and tensile strengths than the V-Alloy, it achieved a higher elongation at break. This behavior is attributed to its lower content of strengthening elements such as Cu, Fe, and Cr, as well as the presence of approximately 0.5 wt.% Mn, which stabilizes the formation of $Al_6(Fe,Mn)$ phases that are less detrimental to ductility than $Al_{13}Fe_4$. Both alloys displayed a ductile fracture behavior.
- Although limited to the experiments included in this study, the cradle-to-gate CO_2 emissions for the scrap-based Re-Alloy powders were reduced by approximately 50%, from 31.5 ± 1.8 $kgCO_2/kg$ for the V-Alloy to 15.5 ± 1.0 $kgCO_2/kg$ for the Re-Alloy. This reduction underscores the significant environmental benefits of using recycled and scrap materials in powder production.
- The carbon footprint of the PBF-LB/M process itself was determined to be 15.2 ± 1.2 $kgCO_2/kg$ of deposited material, with no significant differences observed between the two alloys. This finding suggests that, for virgin alloys, the impact of powder production can dominate the overall environmental footprint.

Overall, this study presented a comprehensive framework for assessing the integration of metal powder production from recycled and scrap materials into PBF-LB/M processes, considering technical feasibility, material processability, and environmental impact. The findings provide a foundation for process optimization and may contribute to the development of more sustainable additive manufacturing strategies. Future work could include advanced numerical modeling and theoretical approaches to deepen the understanding of melt pool behavior, including heat transfer and solidification phenomena. This would enhance the fundamental knowledge of laser–material interactions and support the optimization of processing parameters for additive manufacturing using recycled metallic powders, which may exhibit varying absorptivity due to surface oxidation or compositional differences. In addition, future studies should focus on assessing the reproducibility and reliability of scrap-derived powders by analyzing multiple production batches. Particular attention should be given to the consistency of chemical composition and the influence of trace impurities on material performance. Systematic EDX and statistical analyses could help validate the quality of recycled feedstock and ensure their suitability for high-performance industrial applications.

CRediT authorship contribution statement

Chiara Monti: Writing – review & editing, Writing – original draft, Visualization, Validation, Methodology, Investigation, Conceptualization. **Federico Simone Gobber:** Writing – original draft, Validation, Methodology, Investigation. **Matteo Turani:** Methodology, Investigation. **Konrad Papis:** Writing – review & editing, Supervision, Funding acquisition. **Paolo C. Priarone:** Writing – review & editing, Writing – original draft, Methodology, Investigation, Conceptualization. **Marco Actis Grande:** Writing – review & editing, Supervision. **Markus Bambach:** Writing – review & editing, Supervision.

Declaration of competing interest

The authors declare the following financial interests/personal relationships which may be considered as potential competing interests: Chiara Monti reports financial support provided by Innosuisse Swiss Innovation Agency. Chiara Monti, Matteo Turani, Konrad Papis, Markus Bambach has patent #EP4438752A1 pending to GF Casting Solutions AG. The other authors declare that they have no known competing financial interests or personal relationships that could have appeared to influence the work reported in this paper.

Data availability

Data will be made available on request.

References

[1] S.-S. Li, X. Yue, Q.-Y. Li, H.-L. Peng, B.-X. Dong, T.-S. Liu, H.-Y. Yang, J. Fan, S.-L. Shu, F. Qiu, et al., Development and applications of aluminum alloys for aerospace industry, J. Mater. Res. Technol. 27 (2023) 944–983.
[2] D. Raabe, D. Ponge, P.J. Uggowitzer, M. Roscher, M. Paolantonio, C. Liu, H. Antrekowitsch, E. Kozeschnik, D. Seidmann, B. Gault, et al., Making sustainable aluminum by recycling scrap: The science of dirty alloys, Prog. Mater. Sci. 128 (2022) 100947.
[3] J.L. Cann, A. De Luca, D.C. Dunand, D. Dye, D.B. Miracle, H.S. Oh, E.A. Olivetti, T.M. Pollock, W.J. Poole, R. Yang, et al., Sustainability through alloy design: Challenges and opportunities, Prog. Mater. Sci. 117 (2021) 100722.
[4] T.G. Gutowski, S. Sahni, J.M. Allwood, M.F. Ashby, E. Worrell, The energy required to produce materials: constraints on energy-intensity improvements, parameters of demand, philosophical transactions of the royal society a: Mathematical, Phys. Eng. Sci. 371 (1986) (2013) 20120003.
[5] P.A. Rometsch, Y. Zhu, X. Wu, A. Huang, Review of high-strength aluminium alloys for additive manufacturing by laser powder bed fusion, Mater. Des. 219 (2022) 110779.
[6] S. Graziosi, J. Faludi, T. Stanković, Y. Borgianni, N. Meisel, S.I. Hallstedt, D.W. Rosen, A vision for sustainable additive manufacturing, Nat. Sustain. (2024) 1–8.
[7] P.C. Priarone, G. Ingarao, Towards criteria for sustainable process selection: On the modelling of pure subtractive versus additive/subtractive integrated manufacturing approaches, J. Clean. Prod. 144 (2017) 57–68.
[8] C. Van Sice, J. Faludi, Comparing environmental impacts of metal additive manufacturing to conventional manufacturing, Proc. Des. Soc. 1 (2021) 671–680.
[9] J. Faludi, M. Baumers, I. Maskery, R. Hague, Environmental impacts of selective laser melting: do printer, powder, or power dominate? J. Ind. Ecol. 21 (S1) (2017) S144–S156.

[10] P.C. Priarone, V. Lunetto, E. Atzeni, A. Salmi, Laser powder bed fusion (l-pbf) additive manufacturing: On the correlation between design choices and process sustainability, Procedia Cirp 78 (2018) 85–90.
[11] D. Raabe, C.C. Tasan, E.A. Olivetti, Strategies for improving the sustainability of structural metals, Nature 575 (7781) (2019) 64–74.
[12] L. Cordova, T. Bor, M. de Smit, S. Carmignato, M. Campos, T. Tinga, Effects of powder reuse on the microstructure and mechanical behaviour of al–mg–sc–zr alloy processed by laser powder bed fusion (lpbf), Addit. Manuf. 36 (2020) 101625.
[13] I. Smolina, K. Gruber, A. Pawlak, G. Ziółkowski, E. Grochowska, D. Schob, K. Kobiela, R. Roszak, M. Ziegenhorn, T. Kurzynowski, Influence of the alsi7mg0. 6 aluminium alloy powder reuse on the quality and mechanical properties of lpbf samples, Materials 15 (14) (2022) 5019.
[14] U. Tradowsky, J. White, R. Ward, N. Read, W. Reimers, M. Attallah, Selective laser melting of alsi10mg: Influence of post-processing on the microstructural and tensile properties development, Mater. Des. 105 (2016) 212–222.
[15] H. Asgari, C. Baxter, K. Hosseinkhani, M. Mohammadi, On microstructure and mechanical properties of additively manufactured alsi10mg_200c using recycled powder, Mater. Sci. Eng.: A 707 (2017) 148–158.
[16] S. Cacace, V. Furlan, R. Sorci, Q. Semeraro, M. Boccadoro, Using recycled material to produce gas-atomized metal powders for additive manufacturing processes, J. Clean. Prod. 268 (2020) 122218.
[17] M. Benedetti, M. Perini, M. Vanazzi, A. Giorgini, G. Macoretta, C. Menapace, Atomized scrap powder feedstock for sustainable inconel 718 additive manufacturing via lpbf: a study of static and fatigue properties, Prog. Addit. Manuf. 9 (6) (2024) 1843–1856.
[18] B.-M. Moon, J.H. Seo, H.-J. Lee, K.H. Jung, J.H. Park, H.-D. Jung, Method of recycling titanium scraps via the electromagnetic cold crucible technique coupled with calcium treatment, J. Alloys Compd. 727 (2017) 931–939.
[19] C. Monti, M. Turani, K. Papis, M. Bambach, A new al-cu alloy for lpbf developed via ultrasonic atomization, Mater. Des. 229 (2023) 111907.
[20] V. Tebaldo, G. Gautier di Confiengo, D. Duraccio, M.G. Faga, Sustainable recovery of titanium alloy: From waste to feedstock for additive manufacturing, Sustainability 16 (1) (2023) 330.
[21] F.S. Gobber, P.C. Priarone, A. Pennacchio, M.A. Grande, Effect of inert gas pressure on the properties and carbon footprint of uns s32760 powders made from waste materials by gas atomization, J. Mater. Res. Technol. 33 (2024) 8814–8828.
[22] M. Balbaa, A. Ghasemi, E. Fereiduni, M. Elbestawi, S. Jadhav, J.-P. Kruth, Role of powder particle size on laser powder bed fusion processability of alsi10mg alloy, Addit. Manuf. 37 (2021) 101630.
[23] ISO, 14040 International Standard, Environmental Management—Life Cycle Assessment—Principles and Framework, Second ed.
[24] ISO, 14044 International Standard, Environmental Management—Life Cycle Assessment—Requirements and Guidelines, First ed.
[25] ISO, 14067 International Standard, Greenhouse Gases—Carbon Footprint of Products—Requirements and Guidelines for Quantification, First ed.
[26] European Commission—Joint Research Centre, International Reference Life Cycle Data System (ILCD) Handbook - General guide for Life Cycle Assessment - Detailed guidance, 2010, First edition March 2010. EUR 24708 EN. Luxembourg. Publications Office of the European Union.
[27] L. Zampori, R. Pant, Suggestions for updating the Product Environmental Footprint (PEF) method, Publ. Off. Eur. Union: Luxemb. JRC Technical Reports - European Commission (2019) http://dx.doi.org/10.2760/424613.
[28] V. Pusateri, M.Z. Hauschild, S. Kara, C. Goulas, S.I. Olsen, Quantitative sustainability assessment of metal additive manufacturing: A systematic review, CIRP J. Manuf. Sci. Technol. 49 (2024) 95–110.
[29] M.J. Balart, J.B. Patel, Z. Fan, Melt protection of mg-al based alloys, Metals 6 (6) 131.
[30] S.E. Brika, M. Letenneur, C.A. Dion, V. Brailovski, Influence of particle morphology and size distribution on the powder flowability and laser powder bed fusion manufacturability of ti-6al-4v alloy, Addit. Manuf. 31 (2020) 100929.
[31] B. Brandau, A. Da Silva, C. Wilsnack, F. Brueckner, A.F. Kaplan, Absorbance study of powder conditions for laser additive manufacturing, Mater. Des. 216 (2022) 110591.
[32] M. Ceroni, F.S. Gobber, M. Actis Grande, Ultraviolet–visible-near infrared spectroscopy for assessing metal powder cross-contamination: A multivariate approach for a quantitative analysis, Mater. Des. 242 (2024) 113023.
[33] Granta Design Limited, CES Selector V. 17.2.0, Update 1, Granta Design Limited, UK, 2017.
[34] A. Azapagic, D. Amienyo, R.M. Cuéllar Franca, H.K. Jeswani, Carbon footprints of recycled solvents - study for the european solvent recycler group (esrg), 2013, http://www.ethosresearch.co.uk (Accessed 17 December 2024).
[35] European Solvents Industry Group (ESIG), Eco-profile of three oxygenated solvent (groups): n-butanol, butyl glycol ethers, acetone, 2021, http://www.esig.org. (Accessed 17 December 2024).
[36] European Environment Agency (EEA), Greenhouse gas emission intensity of electricity generation, country level, 2024, https://www.eea.europa.eu/en/analysis/indicators/greenhouse-gas-emission-intensity-of-1/greenhouse-gas-emission-intensity-of-electricity-generation-country-level. (Accessed 17 December 2024).
[37] K. Kellens, M. Baumers, T.G. Gutowski, W. Flanagan, R. Lifset, J.R. Duflou, Environmental dimensions of additive manufacturing: mapping application domains and their environmental implications, J. Ind. Ecol. 21 (S1) (2017) S49–S68.
[38] A. Ghasemi, E. Fereiduni, M. Balbaa, S.D. Jadhav, M. Elbestawi, S. Habibi, Influence of alloying elements on laser powder bed fusion processability of aluminum: A new insight into the oxidation tendency, Addit. Manuf. 46 (2021) 102145.
[39] R. Cunningham, C. Zhao, N. Parab, C. Kantzos, J. Pauza, K. Fezzaa, T. Sun, A.D. Rollett, Keyhole threshold and morphology in laser melting revealed by ultrahigh-speed x-ray imaging, Science 363 (6429) (2019) 849–852.
[40] C. Monti, M. Turani, S. Wierschke, K. Papis, M. Bambach, Microstructure and mechanical properties of alticrfe and alticrcu alloys processed by laser powder bed fusion, Mater. Sci. Eng.: A 892 (2024) 146035.
[41] W. Wang, N. Takata, A. Suzuki, M. Kobashi, M. Kato, Design of Al–Fe–Mn alloy for both high-temperature strength and sufficient processability of laser powder bed fusion, Addit. Manuf. 68 (2022) (2023) 103524, http://dx.doi.org/10.1016/j.addma.2023.103524.
[42] W. Wang, Y. Xu, M. Deguchi, N. Takata, A. Suzuki, M. Kobashi, M. Kato, M. Mitsuhara, H. Nakashima, Thermal stability of refined Al6(Fe, Mn) phase formed in laser powder bed fusion process, J. Alloys Compd. 992 (2024) 174593, http://dx.doi.org/10.1016/j.jallcom.2024.174593.
[43] L. Li, T. Yuan, B. Feng, The microstructures and mechanical properties of al-zn-mg-cu-si-zr alloy: a comparison between directed energy deposition and laser powder bed fusion, Mater. Lett. 337 (2023) 133959.
[44] S. Rech, A. Trentin, S. Vezzu, E. Vedelago, J.-G. Legoux, E. Irissou, Different cold spray deposition strategies: single-and multi-layers to repair aluminium alloy components, J. Therm. Spray Technol. 23 (2014) 1237–1250.
[45] D. Karlsson, G. Lindwall, A. Lundbäck, M. Amnebrink, M. Boström, L. Riekehr, M. Schuisky, M. Sahlberg, U. Jansson, Binder jetting of the alcocrfeni alloy, Addit. Manuf. 27 (2019) 72–79.
[46] H. Zou, Y. Sun, M. Chen, Y. Jiang, Y. Fu, H. Xiong, L. Zhang, K. Zhou, Microstructure and mechanical property of high-density 7075 al alloy by compression molding of pom-based feedstock, J. Mater. Res. Technol. 32 (2024) 4387–4399.
[47] J.H. Martin, J.E. Barnes, K.A. Rogers, J. Hundley, D.L. LaPlant, S. Ghanbari, J.-T. Tsai, D.F. Bahr, Additive manufacturing of a high-performance aluminum alloy from cold mechanically derived non-spherical powder, Commun. Mater. 4 (1) (2023) 39.
[48] IperionX, Comparative life cycle assessment of IperionX 100% recycled spherical titanium powder compared to other spherical metal powders for additive manufacturing, 2024, ABN 84 618 935 372 (accessed December 17 2024).